processes

MDPI

Article

Research on *Camellia oleifera* Shell Mechanical–Structural Cracking Behavior During Collision Hulling with In Situ Testing

Honggen Xing [1], Liu Yang [2,3,*], Menghao Zhao [2,*], Zhide Ma [1], Zhicheng Wang [2], Can Shu [2], Pingan Huang [2] and Bo Cui [2]

[1] School of Machinery and Automation, Zhixing College of Hubei University, Wuhan 430011, China
[2] College of Mechanical Engineering, Wuhan Polytechnic University, Wuhan 430048, China
[3] Hubei Cereals and Oils Machinery Engineering Center, Wuhan 430048, China
* Correspondence: yangliuvictry@whpu.edu.cn (L.Y.); menghz2929868@163.com (M.Z.)

Abstract: Shelling *Camellia oleifera* fruit (COF) is a fundamental step in its oil extraction and further processing. Mechanical shelling mainly relies on cracking through collision. Determining the collision mechanics and structural damage to COF during shelling under specific conditions is crucial for the design of the shelling equipment. In this study, a self-established COF collision mechanical–structural cracking damage test platform was built, with observation in situ using a high-speed macro camera. The main influencing factors on the impact force and structural damage during shelling were analyzed in depth, including the collision material, position, drying temperature, and impact angle. The experimental test results show that the COF collision cracking behavior can be divided into two stages—initial contact to maximum deformation, cracking, and propagation—matching with the mechanical–structural testing. Collision along the *y*-axis obviously causes more damage than that along the *x*-axis. Cracking of the COF occurs when the impact speed exceeds 3.27 m/s. The collision materials 304 stainless steel and 7075 aluminum alloy significantly facilitate cracking, while fresh fruit and polyurethane as collision materials cause no obvious damage. The drying temperature reduces the shell-breaking force for COF, with a drying temperature of 110° leading to the best shell-breaking. This research identifies key factors influencing the cracking behavior in COF shelling, such as the material selection, impact speed, and drying temperature. Optimizing these parameters can enhance shelling efficiency, reduce equipment wear, and increase throughput. This tailored approach supports scalable, cost-effective, and high-quality COF oil production with minimized waste and energy use.

Keywords: *Camellia oleifera* fruit; collision; shelling; crack mechanism

check for updates

Academic Editor: Dariusz Dziki

Received: 8 January 2025
Revised: 14 February 2025
Accepted: 15 February 2025
Published: 14 March 2025

Citation: Xing, H.; Yang, L.; Zhao, M.; Ma, Z.; Wang, Z.; Shu, C.; Huang, P.; Cui, B. Research on *Camellia oleifera* Shell Mechanical–Structural Cracking Behavior During Collision Hulling with In Situ Testing. *Processes* **2025**, *13*, 856. https://doi.org/10.3390/pr13030856

Copyright: © 2025 by the authors. Licensee MDPI, Basel, Switzerland. This article is an open access article distributed under the terms and conditions of the Creative Commons Attribution (CC BY) license (https://creativecommons.org/licenses/by/4.0/).

1. Introduction

Camellia oleifera is a woody oil crop with a high seed oil content and the largest cultivation area in China, predominantly grown in southern regions such as Hunan, Jiangxi, and Guangxi, as well as in Southeast Asian countries [1,2]. COF has an irregular round or oval shape [3]. Its seed oil is recognized as a high-quality edible oil by the United Nations FAO [1]. The COF processing chain includes drying, shelling, seed-shell separation, and oil extraction (Figure 1) [4]. Hulling COF shells is a critical step for obtaining its seeds and extracting its oil, as the shell is both environmentally useful and a potential resource for activated carbon and saponin production [5]. Mechanized shelling, primarily relying on collision, extrusion, or cutting, is essential for improving efficiency and reducing

labor [6,7]. However, the structural–mechanical behavior of COF shells during collision hulling remains underexplored, limiting equipment optimization [8].

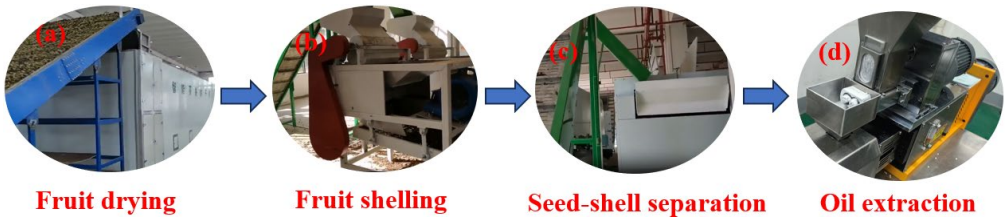


Figure 1. A diagram of *Camellia oleifera* fruit processing. (**a**) Drying. (**b**) Shelling. (**c**) Seed-shell separation. (**d**) Oil extraction.

Related studies highlight key aspects of COF processing. Impact-driven harvesters and flexible rubbing systems have been designed to enhance the shelling efficiency [9,10]. Shell damage is influenced by uneven pericarp shrinkage during dehydration, which facilitates seed-shell separation [11]. Axial and longitudinal loading experiments reveal stress concentration at the pericarp junctions, with radial extrusion promoting rupture [12]. Temperature plays a dual role: high-temperature drying accelerates cracking, but is a risk to seed quality, while low-temperature airflow drying (20–50 °C) achieves 100% cracking rates with minimal energy consumption [13,14]. Despite this progress, the structural–mechanical properties of COF shells under dynamic collision conditions—which are critical for designing efficient shelling equipment—are poorly understood [15].

COF processing includes four main steps: pretreatment, shelling, shell-seed separation, and extraction [16]. During pretreatment, the COF is first piled up, the moisture content in the air is reduced, and part of the naturally split seeds is obtained. About 10 days of airing is needed to convert organic substances (starch and soluble sugars) into oil [17]. Findings have indicated that piling up enhances the post-maturity of *Camellia oleifera* seeds, causing a slow reduction in the moisture levels, along with an initial rise in the oil content that eventually plateaus [18]. During shelling, COF is shelled under mechanical interactions. A common shelling method is pericarp popping. Shelling through popping the pericarps occurs due to uneven pericarp shrinkage strain after dehydration. Uneven pericarp shrinkage is the main driving force behind uncoupling of the seeds and pericarp [19]. During shell-seed separation, the shell-seed mixture from shelling is further refined. Techniques such as vibration sieving are employed to isolate the seeds from residual shell fragments. This step ensures seed purity, minimizes shell residue, and improves oil quality. During extraction, Camellia oil is extracted from seeds separated from the shell-seed mixture after shelling [20]. COF shelling requires pretreatment to achieve a high shelling rate, which finally leads to high-quality oil extraction. This is a basic research aspect for COF processing lines [21].

This study addresses this gap by establishing an in situ testing platform to analyze COF shell cracking behavior during collision. Key factors, such as the collision material, position, impact angle, and drying temperature, are systematically investigated. The findings aim to optimize the shelling parameters (e.g., impact speed, material selection) to enhance efficiency, reduce equipment wear, and support scalable, sustainable oil production.

2. Materials and Methods

2.1. Experimental Materials

The maturity period of COF is commonly in autumn [22]. The COFs used in the experiment were all picked in Yongzhou, Hunan province in October 2024. COF is composed of a shell, seed, and columnal core [23]. The seed is hexagonal or diamond-shaped, and it is plump and thick. The split fruit shell resembles small leaves, with sharp corners at

each end and uneven thickness. As shown in Figure 2b, the part near the branch root is thinner (about 2–3 mm), while the top part is thicker (about 4–5 mm). COF size and mass were measured with a vernier caliper and an electronic scale and classified before the collision test, to reduce the influence of sample differences on the experimental results. COF samples with a nondestructive surface and a transverse diameter of 27–29 mm were selected. The fruits' moisture content was 60–70% [24]. All samples were stored in a temperature and humidity chamber at 4 °C (KH WS-400, Kenton, Guangzhou, China). The longitudinal direction of a COF is defined as the *y*-axis, and the transverse direction as the *x*-axis. Positions at one-quarter and one-half of the COF were defined for analyzing the crack results in subsequent tests, as shown in Figure 2a.

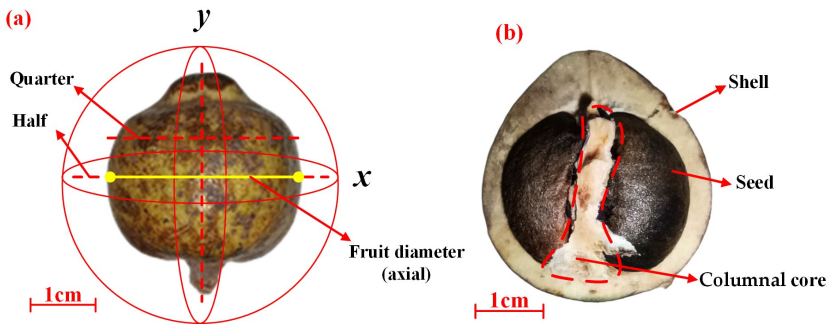


Figure 2. Diagram of overall shape and internal structure of *Camellia oleifera* fruit. (**a**) Overall shape diagram and position definition. (**b**) Internal structure diagram.

The collision materials used during COF postharvest processing included fresh fruit, polyurethane, 7075 aluminum alloy, and 304 stainless steel. Fresh fruit was selected from the same batch of samples, while polyurethane, 7075 aluminum alloy, and 304 stainless steel were purchased from the market. The properties of these collision materials are shown in Table 1.

Table 1. Collision material properties.

Material	Hardness (HV)	Elastic Modulus (GPa)	Density (g/cm^3)
Fresh fruit	2.5	0.01	1.05
Polyurethane	85	0.03	1.20
7075 aluminum alloy	175	71.7	2.81
304 stainless steel	215	193	8.00

2.2. Experiment

A collision damage testing device was established to investigate the COF shell mechanical–structural cracking behavior, and the schematic diagram and testing scenario are shown in Figure 3. The self-established device is mainly composed of a collision device (collision rod and chuck), a data acquisition–processing device (force sensor and computer), and in situ high-speed observation device (high-speed camera and light source); a force sensor (CZL-2BTJH-2B, Xi'an Xinmin Sensor Co., Ltd., Xi'an, China) is installed on the collision platform side. The collision process was recorded at 2000 fps, with a resolution of 800 × 600 pixels, using a high-speed camera (Qianlilang RF-SH6-109, Shenzhen Shenshi Intelligent Technology Co., Ltd., Shenzhen, China) [25]. The camera was positioned 30 cm above the collision platform, aligned orthogonally to the COF's longitudinal axis (*y*-axis), to capture real-time deformation and crack initiation. A diffused LED light source (1000 lux) was installed at 45° to the collision plane to ensure uniform illumination.

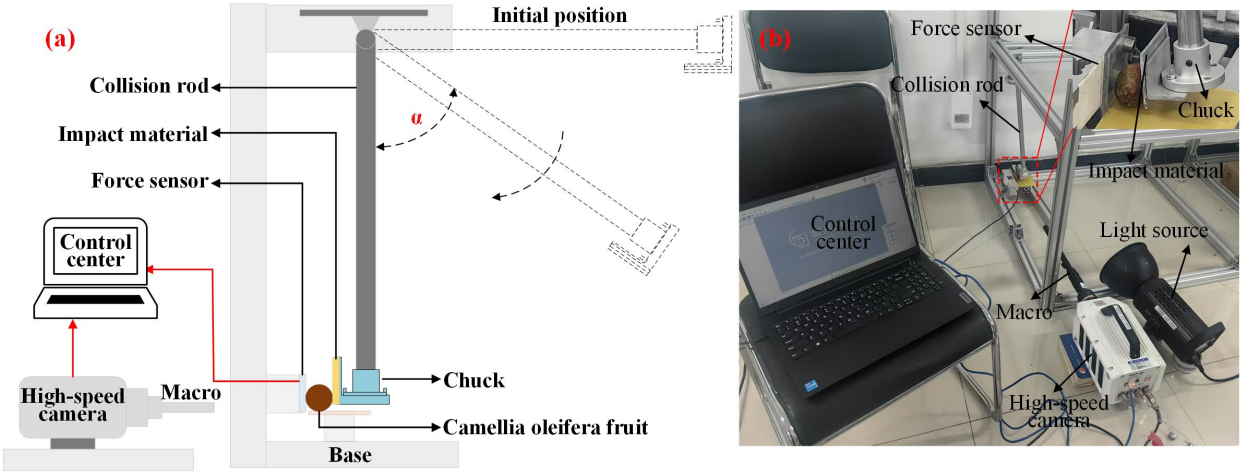


Figure 3. Self-established impact device: (**a**) schematic diagram and (**b**) testing scenario.

The COF impact-based shelling behavior was researched under the influence of several factors: collision position, impact angle (determined according to the angle at which the collision rod was lifted in the experimental device), collision material, and drying temperature. The collision positions included the quarter position, half position, and locations along the *x*-axis and *y*-axis of the COF, as shown in Figure 4. The impact angle was set at 30°, 50°, 70°, and 90°, to cover a range from low- to high-impact angles. Fresh fruit, polyurethane, 7075 aluminum alloy, and 304 stainless steel were selected as collision materials to evaluate the impact of material properties (hardness and elasticity) on the shelling effect. The drying temperature was set at 20 °C, 50 °C, 80 °C, and 110 °C to study the effect of temperature on the shell structure and shelling efficiency of *Camellia oleifera*.

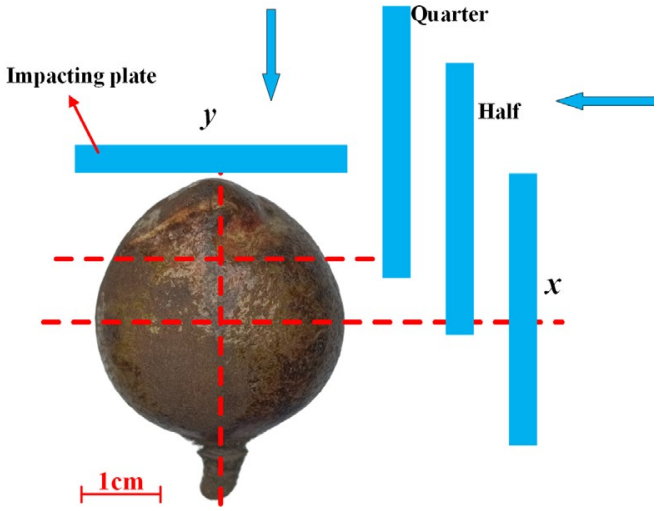


Figure 4. A diagram of the different collision positions.

Before the collision testing, the COF samples were placed horizontally or vertically on the collision platform. The high-speed in situ observation equipment was adjusted to make it focus on the COF. The acquisition frame rate was set to 2000 frames per second, and the acquisition duration was set to 1000 milliseconds. The angle of the collision rod was adjusted through the above-mentioned mechanism, and there was an angle measurement device on the side of the collision rod and the frame. During the test, the external triggers for the high-frame-rate in situ observation equipment and the collision rod were activated by the same start button. After pressing the start button, the collision rod would fall freely,

converting the gravitational potential energy into kinetic energy to collide with the COF. The displacement of the collided COF was limited by the force sensor, and the impact force was transmitted to the PC acquisition terminal through the force sensor. The relevant parameters of the collision test platform can be described as follows: the maximum collision height was 0.53 m, the collision rod's weight was 1.233 kg, and the total weight of the chuck and collision material was 0.085 kg.

The impact speed on the COF was controlled by adjusting the angle α between the collision rod and its vertical axis. According to relevant mechanical calculation formulas [26], when the test collision material was added, the speed when it reached the bottom was 1.38 m/s at $\alpha = 30^\circ$; at $\alpha = 50^\circ$, the speed was 2.26 m/s; at $\alpha = 70^\circ$, the speed was 3.07 m/s; and at $\alpha = 90^\circ$, the speed was 3.78 m/s.

3. Results and Discussion

3.1. Mechanical–Structural Properties of Camellia oleifera Fruit During Collision

COF shells' mechanical and structural cracking behavior is closely linked to the impact force–time relationship during collisions. During the COF collision process, the contact and compression time between the collision rod and the COF is short; the whole test recording time is 1s. Under the 7075 aluminum alloy, an impact angle of 90°, and a drying temperature of 20 °C, the COF impact force–time curve and surface image are shown in Figure 5. During the whole collision process, the impact time of the COF was 0.1 s. The curve can be divided into two stages, according to the cracking appearance of the COF. In the first stage, the impact force increases rapidly and is maintained for a short time after reaching its peak, which corresponds to the maximum deformation stage of the COF. The first stage includes initial contact, deformation, and maximum deformation. Initial contact: the COF contacts the collision material surface for the first time; the COF does not deform or show cracking. Deformation: with the impact, the COF begins to deform, and the impact force increases gradually in this process, until it reaches the maximum. Maximum deformation: when the COF reaches its maximum deformation and the impact force peaks, the shell of *Camellia oleifera* remains intact, without cracking. In the second stage, the impact force decreases as cracks form and propagate, until the COF leaves the sensor surface. The second stage includes the appearance of cracks, maximum cracking, and the departure of the COF. Cracks appear: when the impact force reaches its maximum, the shell of the COF begins to show cracking. It is during this period that the crack begins to expand. Maximum cracking: the crack continues to expand until it reaches its maximum size. A wide crack exists in the shell of the COF, and the impact force begins to decline. Departure: the impact force continues to decrease, and the COF finally separates from the sensor surface, marking the end of the impact process.

During the impact test of the 7075 aluminum alloy on the COF, the COF underwent two distinct stages: deformation and recovery deformation. As shown in Figure 5, the force–time curve indicates that deformation was initiated at 15.8 N (point b, onset of measurable compression), and reached its maximum at the peak force of 53.7 N (point c, corresponding to maximum shell deformation). Subsequent force reduction coincided with crack initiation and propagation (point d–e). Subsequently, the impact force began to decrease, and small cracks appeared on the COF shell (point d). As the collision progressed, the cracks expanded and reached their maximum extent (point e). With a further reduction in impact force, the COF started to recover from its deformation, and the cracks gradually diminished (e–f). This process demonstrates a rapid rise in impact force during the initial contact, followed by a gradual decline as cracks form, expand, and close. The test results reveal the dynamic response of COF under impact, including its deformation characteristics and crack evolution behavior.

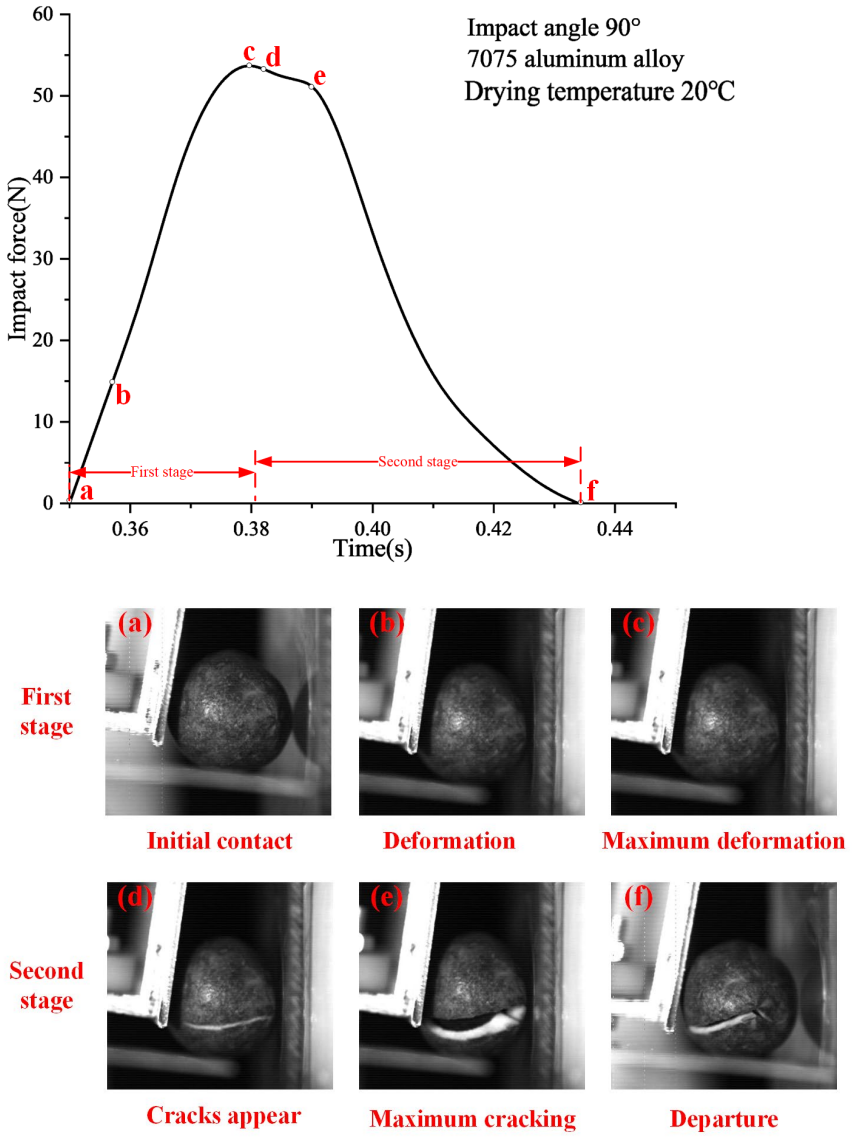


Figure 5. Impact force–time curve and surface image of *Camellia oleifera* fruit. (**a**) Initial contact. (**b**) Deformation. (**c**) Maximum deformation. (**d**) Cracks appear. (**e**) Maximum cracking. (**f**) Departure.

3.2. Influence of Different Collision Positions on Camellia oleifera Fruit Shelling

Due to the COF shell's spatial structure, the shell's mechanical properties differ under different fruit shell collision positions [27]. It is significant to study the shell's rupture at different collision positions during shelling. Under 304 stainless steel, an impact angle of 90°, and a temperature of 20 °C, conducting quarter, half, x, and y collisions, the crack damage under the collision test is shown in Figure 6. The figure indicates that after COF collisions at the half and quarter positions, the damage mainly comprises impact marks on the collision parts, and the predominant crack type is slip cracks. At the quarter position, the fruit shell shows wear-like damage. At the half position, the impact marks are less severe, and the contact area of the fruit shell increases. During the collision in the x and y directions, the COF develops collision cracks in the x direction. This mainly depends on the differences among the fruits and whether the impact area has a crack structure. However, the collision damage in the y direction is much greater than that in the x direction, and fruit shell detachment occurs. This indicates that under the same experimental conditions, the collision in the y direction is more conducive to shelling and

crack behavior. The stress concentration at the top is greater than that of the crack line structure, and cracks will first appear in the top area [28].

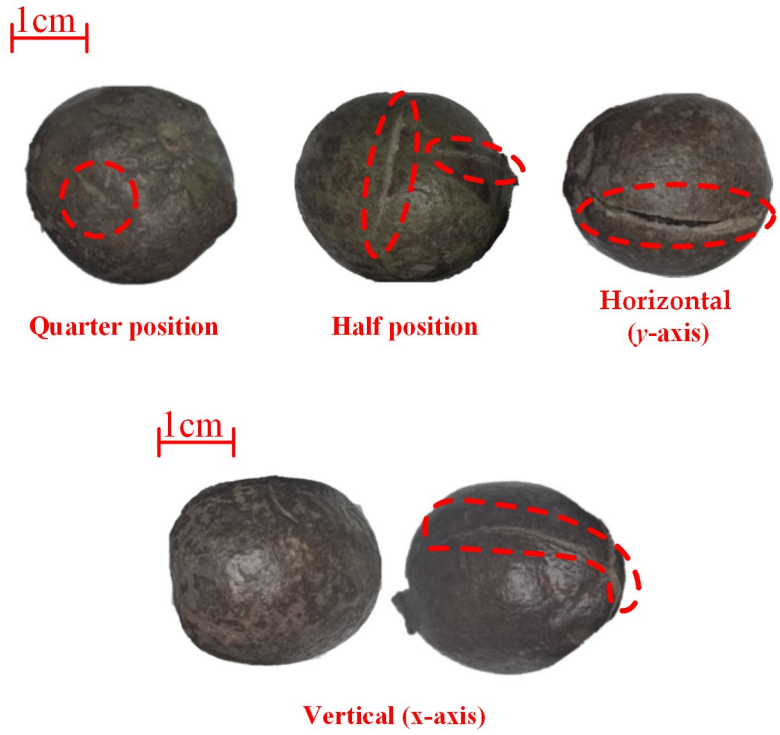


Figure 6. Damage pattern of *Camellia oleifera* fruit under different collision positions.

3.3. Influence of Different Collision Angles on Camellia oleifera Fruit Shelling

Different impact forces affect COF shelling. A smaller impact force can hardly break the fruit shell, whereas a moderate impact force can make the fruit shell crack along its weak parts [29]. Under the impact material of 304 stainless steel and a temperature of 20 °C, the impact angles of the collision test were set to 30°, 50°, 70° and 90°. Based on the experimental data of each collision recorded by the sensor, the impact forces of 304 stainless steel on COF at different impact angles are shown in Figure 7. As the impact angle increases, the impact force against the COF escalates correspondingly. At higher impact angles, the geometric interaction between the collision rod and the curved surface of the fruit reduces the effective contact area. This is inferred from localized deformation patterns observed post-impact, leading to the increased stress on the shell. Under all tested angles, especially at 70° and 90°, the impact force reaches 47.54 ± 3.2 N and 55.66 ± 2.6 N, respectively. Due to the high strength and hardness of steel, high impact force appeared during the test.

The impact material of 304 stainless steel exhibited relatively high impact force under all the tested angles; a detailed analysis was conducted. With stainless steel as the collision material, collision tests at different angles were carried out at room temperature (20 °C), and the high-frame-rate in situ observation equipment was used to measure the speed of the collision part. The measurement results were as follows: under the rod lifting angle of 30°, the speed was 1.42 m/s; under 50°, the speed was 2.35 m/s; under 70°, the speed was 3.27 m/s; and under 90°, the speed was 3.96 m/s.

The COF surface morphology after the collision was observed. As shown in Figure 8, no cracks appeared on the COF surface under the impact angles of 30° and 50°. The impact forces were 20.77 ± 2.5 N and 35.75 ± 2.4 N, respectively; the corresponding collision speeds were 1.42 m/s and 2.35 m/s. Under an impact angle of 70° or above, observable cracking behaviors appeared on the exterior of the COF. The fruit shell reached the shell-breaking force, and crack evolution occurred. The impact forces at the collision angles of

70° and 90° were 47.54 ± 3.2 N and 55.66 ± 2.6 N. A collision damage diagram of COF under different impact angles is shown in Figure 8. Under the impact angle of 70°, the cracks of the COF were in the form of fissures along the *y*-axis. Under the impact angle of 90°, the cracks on the outer shells of the COF spread from the top to the surroundings along the *y*-axis.

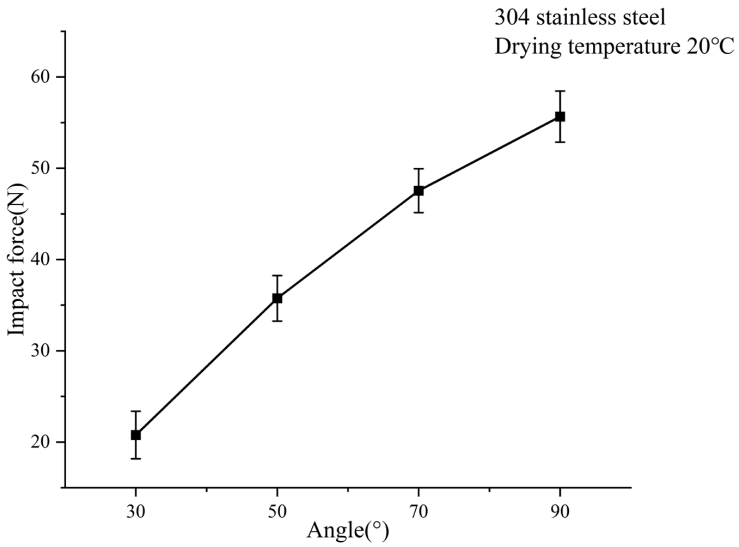


Figure 7. Peak impact force at different angles.



Figure 8. Collision damage diagram of COF under different collision angles.

The COF shell-breaking force is 218.5 ± 60.3 N under quasi-static compression conditions [23]. This indicates that the breaking force under impact conditions is much smaller than the shelling force of the fruit shells. Based on the static pressure experiment, the shell-breaking force of the fruit shells is affected by the compression speed; a larger compression speed will reduce the shell-breaking force. The formation of cracks in COF is not solely dependent on the impact speed of the tip, but is also significantly influenced by the mass of the pendulum. For a given impact speed, a larger pendulum mass will result in greater collision energy, thus causing cracks to occur at lower speeds. Conversely, for a smaller pendulum mass, cracks will occur at higher speeds. This provides important insights for subsequent optimization of shelling equipment. The experimental results show that under the specific conditions of the device (with a pendulum mass of 1.233 kg), COF cracking is observed when the impact speed exceeds 3.27 m/s.

3.4. Influence of Different Collision Materials on Camellia oleifera Fruit Shelling

Collision working components with different materials significantly influence the dehulling process [30], playing a crucial role in enhancing shelling efficiency and reducing damage. Under an impact angle of 90° and a drying temperature of 20 °C, fresh fruits,

polyurethane, 7075 aluminum alloy, and 304 stainless steel were used as collision materials to conduct collision tests on the horizontally placed COF samples. The impact forces are shown in Figure 9. In the collision test, when 304 stainless steel was used as the collision material, it produced the highest impact force of 55.75 ± 1.8 N, while when polyurethane was used as the collision material, it produced the lowest impact force of 52.46 ± 2.1 N. Due to the high hardness and strong rigidity of 304 stainless steel [31], it is not easy to deform during collision, and hardly absorbs any collision energy. Its surface is smooth and hard, with a short contact time and a concentrated impact force. Coupled with its high density, large mass, and great inertia, it leads to a large impact force generated by the collision. Polyurethane has relatively low hardness and is elastic [32]. During collision, it can buffer the collision energy through its deformation, and its internal molecular structure can store and dissipate energy. Its relatively soft surface results in a large contact area and a long contact time; the impact force transmitted to the COF is relatively small.

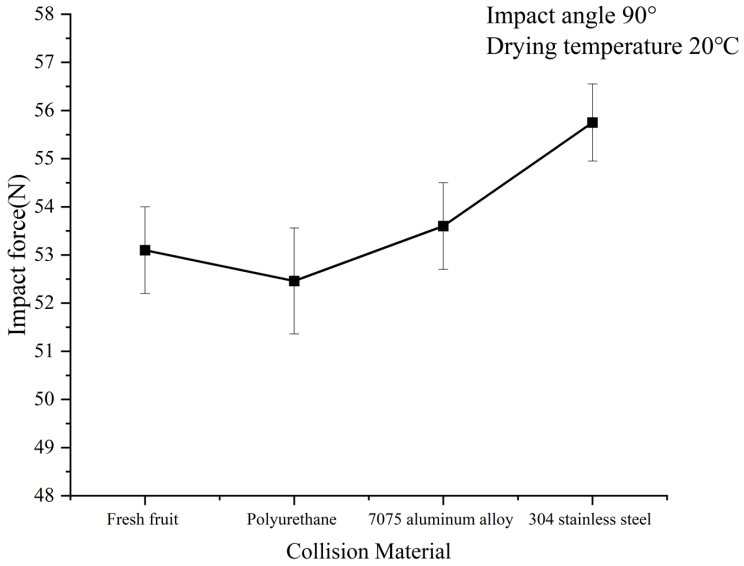


Figure 9. Peak impact force under different collision materials.

The collision results under different collision materials are shown in Figure 10. The 304 stainless steel and 7075 aluminum alloy had a significant impact on the collision cracks of COF. Fresh fruits and polyurethane did not cause cracking of the fruit shells during the collision process. This indicates that during the shelling process of COF, shelling depends on the force exerted on the fruits by the collision materials, rather than the mutual impact between fruits. This evinces the need for fruits to possess sufficient kinetic energy to achieve impact damage. The peak impact force of 304 stainless steel (55.75 ± 1.8 N) and 7075 aluminum alloy (53.21 ± 2.3 N) was significantly higher than that of polyurethane (52.46 ± 2.1 N) and fresh fruit (51.89 ± 2.4 N) (ANOVA, $p < 0.001$). A Tukey test showed that the impact force of the metal materials (stainless steel, aluminum alloy) and non-metal materials (polyurethane, fruit) was significantly different ($p < 0.01$), but there was no significant difference between the metal materials. The crack observation results indicate that the hardness and low-energy buffering properties of metal materials as the collision material are more likely to cause shell cracking. The finding verifies the application of metal materials in actual shelling.

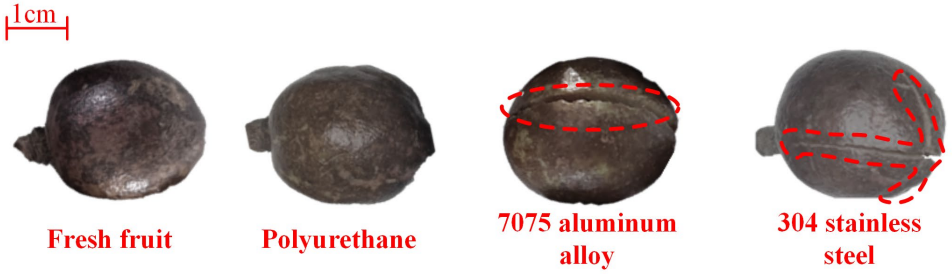


Figure 10. Collision damage diagram of COF under different collision materials.

3.5. Influence of Drying Temperature on Camellia oleifera Fruit Shelling

Drying is an important process for shelling. The effect of drying temperature was investigated for highly efficient shelling work [33]. COF sample collision tests were conducted on a self-established test setup under fruit drying at 20 °C, 50 °C, 80 °C, and 110 °C, with an impact angle of 90°, and stainless steel as the collision material. The tests were repeated at least five times. Fruit samples were dried in an electronic drying oven (JC-9070A, Foshan Nanbeichao E-commerce Co., Ltd., Foshan, China) under the chosen temperature for 0.5 h before tests were conducted. The impact forces are shown in Figure 11.

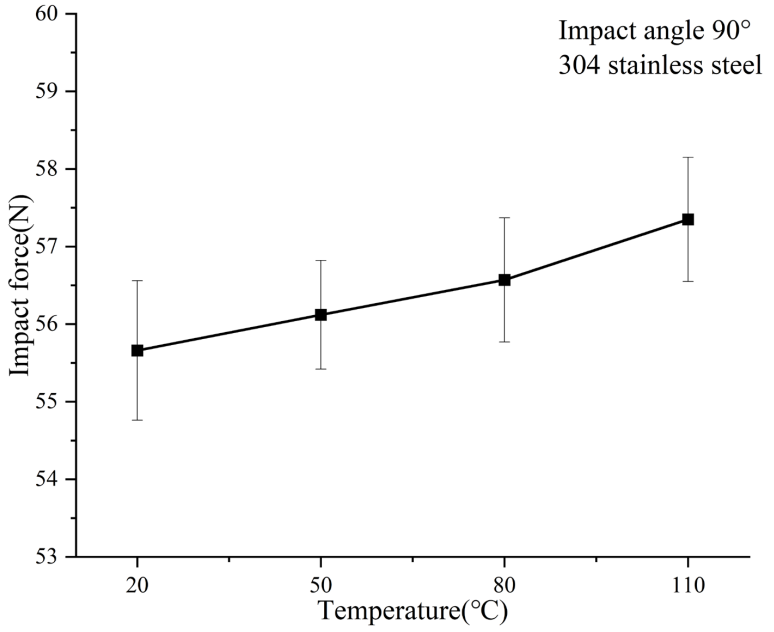


Figure 11. Peak impact force under different drying temperatures.

The impact peak force reached the highest value of 57.35 ± 0.8 N at the drying temperature of 110 °C, indicating that temperature has a significant impact on the structure of COF. At the temperature of 20 °C, the structure of the COF is relatively hard, and a certain amount of force is required during collision. The low temperature keeps the moisture and cell structure inside the fruit stable [34]. When the temperature is medium, in the range of 50–80 °C, the peak impact force increases slightly at 50 °C. The loss of moisture causes changes in the internal substances of the fruit, which makes the shell brittle. When the temperature reaches 80 °C, the force increases again, due to the loss of water reducing the turgor pressure inside the cells, and the cells lose their original plump state [35]. At a high temperature of 110 °C, the peak impact force increases significantly. Due to the reduction in moisture, forces such as hydrogen bonds between components like cellulose and hemicellulose in the cell walls are strengthened, making the cell walls harder and more compact, thereby improving the mechanical strength and hardness of the fruit shells [29].

Temperature affects the energy absorption and transfer during the collision, resulting in a continuous increase in the impact force.

The collision damage is shown in Figure 12. It indicates that as the temperature increases, the crack behavior becomes more and more significant. When the drying temperature is at 50 °C or below, the cracks extend and spread along the crack line structure. At 80 °C, external cracks appear in areas outside of the crack line structure on the fruit shells. This indicates significant changes in the microstructure of the fruit shells, reducing the critical force required for crack development. At 110 °C, the fruit shells are almost shelled off after collision. Judging from the microstructure of the fruit shells, obvious void structures appear in the fruit shell tissues under the influence of temperature. Additionally, the cells lose water and solidify. These changes weaken the elastic deformation ability of the fruit shells and increase their hardness [36]. This is due to the internal cracks in the crack line structure expanding. COF treated at high temperatures shows a better cracking effect during the collision process; temperature is the optimal influencing factor for shelling under collision. Ignoring the influence of factors such as fruit size, drying can increase the shelling rate of COF.

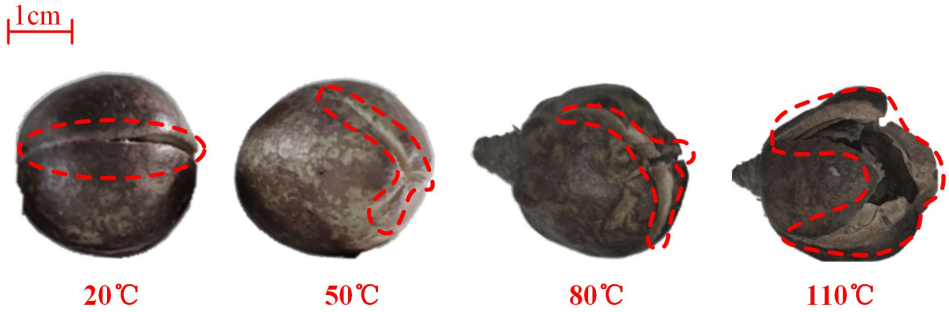


Figure 12. Collision damage diagrams of COF under different drying temperatures.

4. Conclusions

In this study, a collision damage testing device was established to investigate the mechanical–structural cracking behavior of COF shells during collisions. The effects of collision positions, impact angle, collision material, and drying temperature on COF cracking were investigated. The results of COF collision tests show that the COF experiences two stages: deformation and recovery deformation. The first stage includes initial contact, deformation, and maximum deformation. The second stage includes the appearance of cracks, maximum cracking, and departure. Different collision positions were found to affect COF shelling. The collision damage in the y direction was much greater than that in the x direction, and the phenomenon of fruit shell detachment occurred. By converting the collision angles into collision speeds, we found that that COF will not show cracking behavior when the speed is below 3.27 m/s, while external cracks will occur when the speed is above 3.27 m/s. The collision material significantly influenced the crack behavior of the fruit shell during the impact process. Combined with the crack observation results, the hardness and low-energy buffer characteristics of metal materials are more likely to cause shell cracking, which verifies their application advantages in actual shelling equipment. Drying temperature significantly influences the COF shelling process. A higher drying temperature reduces the COF shell-breaking force; a drying temperature of 110° leads to the best shell-breaking.

Based on the findings of this study, future work should focus on expanding the scope of the collision materials tested, to identify optimal options for maximizing shelling efficiency while minimizing seed damage. Efforts should be made to scale up the experimental setup for industrial applications, incorporating the optimal parameters, such as the speed

of the working elements (guided by collision energy thresholds), materials, and drying temperatures, identified in this study. Notably, the critical speed for cracking observed in this study ($\geq$3.27 m/s) is significantly lower than typical industrial machinery speeds, emphasizing the importance of balancing speed with material hardness and energy transfer efficiency to avoid excessive seed damage. Further research should also investigate the impact of different shelling methods on seed quality and oil extraction efficiency, while integrating advanced monitoring systems into industrial shelling machines to provide real-time feedback and optimize the shelling process. These steps will help to translate the findings into practical applications, enhancing the overall efficiency and effectiveness of *Camellia oleifera* fruit shelling operations.

Author Contributions: H.X.: methodology, analysis, and investigation. L.Y.: conceptualization, resources, supervision, project administration, and funding acquisition. M.Z.: supervision and project administration. Z.M.: methodology and analysis. Z.W.: conceptualization and methodology. C.S.: software and validation. P.H.: analysis and validation. B.C.: conceptualization. All authors have read and agreed to the published version of the manuscript.

Funding: The study is mainly funded by the Youth Project of the Natural Science Foundation of Hubei Province (No. 2022CFB944), the Hubei provincial Grain Bureau Science Project (2023HBLSKJ004), the Science and Technology Research Project of the Hubei Provincial Education Department (No. Q20211609), and the Key R&D plan of Hubei Province (No. 2022BBA0047); part of the research is supported by the Jiangsu Key Laboratory of Advanced Food Manufacturing Equipment and Technology (FM-202103).

Data Availability Statement: The datasets generated and analyzed during the present study are available from the corresponding author upon reasonable request.

Acknowledgments: We express our thanks for the support of the Hubei Cereals and Oils Machinery Engineering Technology Research Center at Wuhan Polytechnic University.

Conflicts of Interest: The authors declare no conflicts of interest.

References

1. Xing, K.-F.; Zou, Y.-J.; Xie, H.-X. Variation in Fruit Traits and Seed Nutrient Compositions of Wild *Camellia oleifera*: Implications for *Camellia oleifera* Domestication. *Horticulturae* **2024**, *10*, 450. [CrossRef]
2. Liu, J.; Wu, L.; Chen, D. Development of a soil quality index for *Camellia oleifera* forestland yield under three different parent materials in Southern China. *Soil Tillage Res.* **2018**, *176*, 45–50. [CrossRef]
3. Wang, Y.; Ma, J.; Xiong, R. Design on multi-channel pneumatic planer for *Camellia oleifera* shelling. *Hubei Agric. Sci.* **2018**, *57*, 100.
4. Zhu, G.; Liu, H.; Xie, Y. Postharvest processing and storage methods for *Camellia oleifera* seeds. *Food Rev. Int.* **2020**, *36*, 319–339. [CrossRef]
5. Zhang, J.; Gong, L.; Sun, K. Preparation of activated carbon from waste *Camellia oleifera* shell for supercapacitor application. *J. Solid State Electrochem.* **2012**, *16*, 2179–2186. [CrossRef]
6. Zhang, F.; Zhu, F.; Chen, B. Composition, bioactive substances, extraction technologies and the influences on characteristics of *Camellia oleifera* oil: A review. *Food Res. Int.* **2022**, *156*, 111159. [CrossRef]
7. Ndukwu, M.C.; Asoegwu, S.N. Functional performance of a vertical-shaft centrifugal palm nut cracker. *Res. Agric. Eng.* **2010**, *56*, 77–83. [CrossRef]
8. Ibrahim, A.; Onwualu, A.P. Technologies for extraction of oil from oil-bearing agricultural products: A review. *J. Agric. Eng. Technol.* **2005**, *13*, 58–70.
9. Yan, F.; Li, X.; Huang, G. *Camellia oleifera* fresh fruit harvesting in China. In Proceedings of the 2020 5th International Conference on Mechanical, Control and Computer Engineering (ICMCCE), Harbin, China, 25–27 December 2020; pp. 699–702.
10. Kang, D.; Wang, Y.; Fan, Y. Research and development of *Camellia oleifera* fruit sheller and sorting machine. *IOP Conf. Ser. Earth Environ. Sci.* **2018**, *108*, 042051. [CrossRef]
11. Peng, Y.; Zhou, H.; Zhang, A. Natural products from *Camellia oleifera* fruit and its comprehensive utilisation. *Nat. Prod. Res.* **2024**, *20*, 1–17. [CrossRef]
12. Wei, X.; Chen, X.; Liao, P. Study on the Mechanical Properties and the Way of Breaking the Shell of Fresh *Camellia oleifera* Fruit. *Horticulturae* **2023**, *9*, 236. [CrossRef]

13. Wang, F.; Liu, Z.; Ding, Y. Study on the splitting by hot-air drying of COF. *Int. J. Food Eng.* **2022**, *18*, 143–151. [CrossRef]
14. Jinxiong, L.; Mei'e, Z.; Zhili, W. Low-Temperature Airflow-Drying Cracking Coupling with Flexible Mechanical Deshelling for *Camellia oleifera* Fruit: Process and Mechanism. *Dry. Technol.* **2024**, *42*, 871–879. [CrossRef]
15. Jie, M.; Ang, L.; Xi, L. Structure design of *Camellia oleifera* fruit sheller by EBD method. *IOP Conf. Ser. Earth Environ. Sci.* **2020**, *585*, 012163.
16. Lim, B.Y.; Shamsudin, R.; Baharudin, B. A review of processing and machinery for *Jatropha curcas* L. fruits and seeds in biodiesel production: Harvesting, shelling, pretreatment and storag. *Renew. Sustain. Energy Rev.* **2015**, *52*, 991–1002. [CrossRef]
17. Wu, J.; Fan, X.; Huang, X. Effect of different drying treatments on the quality of *Camellia oleifera* seed oil. *S.Afr. J. Chem. Eng.* **2021**, *35*, 8–13. [CrossRef]
18. Zhu, G.; Lei, D.; Xie, Y. Effects of postharvest piling up in bulk on qualities of *Camellia oleifera* seeds. *J. Stored Prod. Res.* **2024**, *106*, 102291. [CrossRef]
19. Yang, P.; Fu, H.; Sun, P. Shell structure impacts *Camellia oleifera* fruit splitting during dehydration. *Food Bioprod. Process.* **2024**, *148*, 298–308. [CrossRef]
20. Wang, X.; Bian, B.; Tuluhong, T. Experiments and parameter optimization of almond shell and kernel air separation device. *Trans. Chin. Soc. Agric. Eng.* **2021**, *37*, 299–306.
21. Hay, F.R.; Rezaei, S.; Wolkis, D.; McGill, C. Determination andcontrol of seed moisture. *Seed Sci. Technol.* **2023**, *51*, 267–285. [CrossRef]
22. Wen, Y.; Su, S.; Jia, T. Allocation of photoassimilates in bud and fruit from different leaf nodes of *Camellia oleifera*. *HortScience* **2021**, *56*, 469–477. [CrossRef]
23. Yang, L.; Wang, Z.; Cui, B. Experimental and FEM research on *Camellia oleifera* shell structural–mechanical cracking behavior during hulling. *J. Food Process Eng.* **2024**, *47*, e14662. [CrossRef]
24. Zhang, X.; He, C.; Yan, B. Effects of fruit load on growth, photosynthesis, biochemical characteristics, and fruit quality of *Camellia oleifera*. *Sci. Hortic.* **2023**, *317*, 112046. [CrossRef]
25. Tang, H.; Zhu, G.; Wang, Z. Prediction method for maize kernel impact breakage based on high-speed camera and FEM. *Powder Technol.* **2024**, *444*, 120002. [CrossRef]
26. Hinrichsen, P.F. A Simple Moment of Inertia Measurement. *Phys. Teach.* **2022**, *60*, 292–295. [CrossRef]
27. Wang, Q.; Chang, S.; Tan, Y. Mesopore structure in *Camellia oleifera* shell. *Protoplasma* **2019**, *256*, 1145–1151. [CrossRef]
28. Paris, P.C.; Sih, G.C. Stress analysis of cracks. *ASTM Stp* **1965**, *381*, 30–81.
29. Flores-Johnson, E.A.; Carrillo, J.G.; Zhai, C. Microstructure and mechanical properties of hard *Acrocomia mexicana* fruit shell. *Sci. Rep.* **2018**, *8*, 9668. [CrossRef]
30. Singh, S.M.; Rao, P.S. Impact Dehulling of Browntop Millet: Its Physical and Nutritional Characterization. *J. Cereal Sci.* **2024**, *121*, 104078. [CrossRef]
31. Ye, D.; Xu, Y.; Xiao, L. Effects of low-cycle fatigue on static mechanical properties, microstructures and fracture behavior of 304 stainless steel. *Mater. Sci. Eng. A* **2010**, *527*, 4092–4102. [CrossRef]
32. Kogelnik, H.J.; Huang, H.H.; Barnes, M. Comparison of the dynamic properties of solid polyurethane elastomers. *J. Elastomers Plast.* **1991**, *23*, 314–344. [CrossRef]
33. Wang, F.; Guo, C.; Wen, J. Simulation of the splitting process by hot-air drying of *Camellia oleifera* fruit. *Dry. Technol.* **2024**, *42*, 1526–1539. [CrossRef]
34. Wu, L.; Li, J.; Gu, Y. Effect of chilling temperature on chlorophyll florescence, leaf anatomical structure, and physiological and biochemical characteristics of two *Camellia oleifera* cultivars. *Int. J. Agric. Biol.* **2020**, *23*, 777–785.
35. Yang, D.; Pan, S.; Ding, Y. Experimental evidence for negative turgor pressure in small leaf cells of Robinia pseudoacacia L versus large cells of Metasequoia glyptostroboides Hu et WC Cheng. 1. Evidence from pressure—Volume curve analysis of dead tissue. *Plant Cell Environ.* **2017**, *40*, 351–363. [CrossRef]
36. Shang, L.; Yuan, R.; Liu, X. Precursor screening of fruit shell derived hard carbons for low-potential sodium storage: A low lignin content supports the formation of closed pores. *Carbon* **2024**, *223*, 119038. [CrossRef]

Disclaimer/Publisher's Note: The statements, opinions and data contained in all publications are solely those of the individual author(s) and contributor(s) and not of MDPI and/or the editor(s). MDPI and/or the editor(s) disclaim responsibility for any injury to people or property resulting from any ideas, methods, instructions or products referred to in the content.